Nuclear Instruments and Methods in Physics Research A 767 (2014) 318–321

Contents lists available at ScienceDirect

Nuclear Instruments and Methods in Physics Research A

journal homepage: www.elsevier.com/locate/nima

Effects of deep-level defects on carrier mobility in CdZnTe crystals

Lingyan Xu, Wanqi Jie*, Xu Fu, Gangqiang Zha*, Tao Feng, Rongrong Guo, Tao Wang, Yadong Xu, Yasir Zaman

State Key Laboratory of Solidification Processing, School of Materials Science and Engineering, Northwestern Polytechnical University, Xi'an, Shaanxi 710072, China

ARTICLE INFO

Article history:
Received 18 July 2014
Received in revised form
21 August 2014
Accepted 24 August 2014
Available online 6 September 2014

Keywords:
CdZnTe
Scattering mechanism
Carrier mobility
Deep-level defects

ABSTRACT

The effects of deep-level defects on the carrier mobility of $Cd_{0.9}Zn_{0.1}Te$:In single crystals were studied. The total density of donor and acceptor defects in two samples, CZT1 and CZT2, was measured by the thermally stimulated current (TSC) to be $\sim 2.0\times10^{16}\,cm^{-3}$ and $\sim 3.8\times10^{17}\,cm^{-3}$, respectively. The mobility of electrons was measured by time-of-flight (TOF) technique to be $848\pm42\,cm^2/Vs$ in CZT1 and $337\pm17\,cm^2/Vs$ in CZT2. Theoretical estimation of the mobility was made considering the contributions from a variety of scattering mechanisms, including polar-optical phonon scattering, piezoelectric potential scattering, deformation potential scattering and ionized impurity scattering. The total electron mobility was estimated based on Matthiesen's rule to be $1004\,cm^2/Vs$ in CZT1 and $352\,cm^2/Vs$ in CZT2, according to the defect density. Polar-optical phonon scattering was found to be the dominant scattering mechanism limiting the mobility at room temperature when the total defect density is lower than $1.0\times10^{15}\,cm^{-3}$, and ionized impurity scattering will be the dominant when the total defect density higher than $1.0\times10^{17}\,cm^{-3}$.

1. Introduction

Cadmium zinc tellurides (CdZnTe, CZT) have been considered as one of the most promising compound semiconductors for the applications as room-temperature X-ray and γ-ray detectors [1,2]. As-grown CZT crystals generally encounter problems arising from the bulk defects, especially deep-level defects, which would strongly affect the carrier transport properties and the consequent detector performances [3]. Cadmium vacancies have been considered to be the dominant native defects due to the high partial pressure of Cd during crystal growth [4]. Group III (Al, Ga, In) and/or group VII (Cl, Br) dopants can incorporate on Cd sites and introduce donor levels to compensate Cd vacancies [5]. Under tellurium-rich conditions, excess Te in CZT crystals has a maximum solubility of about $4\times10^{18}\,cm^{-3}$ at $\sim$860 °C. The retrograde solubility during the further cooling process will lead to Te precipitations, Te antisites, Te interstitials and Cd vacancy–Te antisite pairs [3,6]. These deep-level defects are responsible for high resistivity by stabilizing the compensation conditions. Meanwhile, they interfere with the carrier transport process and cause incomplete charge collection [7]. Carrier mobility is determined by scattering mechanisms, including polar-optical phonon scattering, piezoelectric potential scattering, acoustic-mode scattering, ionized impurity scattering, neutral impurity scattering, dislocation scattering and so on [8]. This study was aimed at elucidating the nature of the dominant scattering mechanisms and the effects of deep-level defects on the mobility in the carrier transport process.

2. Experimental

$Cd_{0.9}Zn_{0.1}Te$:In single crystals with the dimensions of $10\times10\times1\,mm^3$ were cut from two different ingots grown by the Modified Vertical Bridgman (MVB) method at Imdetek Ltd. The ratio of the raw materials and the doping concentration for the two ingots was the same. However, the detailed crystal growth parameters for them were different, e.g., the temperature field, the growth rate and the cooling rate. Thus, the difference in the crystalline quality and the material property exists in the two ingots. All the samples have n-type conduction with high resistivity of 10^{10}–$10^{11}\,\Omega\,cm$. After polishing and etching, Au electrodes were fabricated on the surfaces using vacuum evaporation deposition. We utilized thermally stimulated current (TSC) measurements to investigate the energy distribution of the deep-level defects. Free carriers excited by achromatic light from a halogen lamp will be captured by defect traps at low temperature. As the temperature increases in the dark from 80 to 320 K at a constant heating rate, trapped electrons and holes released by thermal emission are scanned and recorded under

* Corresponding authors. Tel.: +86 13772439913; fax: +86 29 88495414.
E-mail addresses: jwq@nwpu.edu.cn (W. Jie), zha_gq@hotmail.com (G. Zha).

http://dx.doi.org/10.1016/j.nima.2014.08.040
0168-9002/

an applied bias to obtain the thermally stimulated current. Each peak in the TSC spectrum corresponds to a certain trap level in the band-gap introduced by a certain defect state in the crystal lattice. Time-of-flight (TOF) testing technique was used to investigate the transport properties. Electron-–hole pairs generated by pulsed laser with wavelength of 527 nm and width of 893 ps will drift and induce transient current in the external circuit under an applied bias. The bias was applied using the Keithley 6517 system and the induced current signals were collected using a digital oscilloscope (LecoyWaveRunner 610Zi).

3. Results and discussion

Fig. 1 shows the typical TSC spectra of CdZnTe single crystals. The simultaneous multiple peak analysis (SIMPA) method was adopted to determine trap signatures in TSC spectra [9]. Trap-related parameters, e.g., activation energy, capture cross-section and trap density, were obtained based on the "first-order kinetics" approximation [10,11]. We identified four main traps (T1–T4) in all the samples. The level labeled T1 has an activation energy of 0.06 ± 0.01 eV below the conduction band minimum, with the trap type (electron or hole) revealed by thermoelectric effect spectroscopy (TEES) [12,13]. T1 could be assigned to a shallow donor originated at an In dopant related point defect In_{Cd}^{+} [14,15]. Traps T2 and T3 are recognized as acceptor defects, located at 0.11 ± 0.01 eV and 0.21 ± 0.01 eV above the valence band maximum, respectively. The microscopic origins of these two traps are attributed, respectively, to the firstly and secondly ionized Cd vacancies [15,16]. Trap T4 located at 0.56 ± 0.02 eV below the conduction band minimum could be attributed to the deep donor Te antisite (Te_{Cd}^{2+}) with the second ionization energy of ~0.59 eV [15]. As shown in Table 1, the total density of donor and acceptor defects in CZT2 (3.8×10^{17} cm^{-3}) is one order of magnitude higher than that in CZT1 (2.0×10^{16} cm^{-3}).

Fig. 2 shows the typical transient current waveforms in TOF results measured at different bias voltages. With negative bias applied to the front electrode, the current signals are mainly induced by photo-generated electrons. The drift velocity $v = d/t_{tr}$ determined from current waveforms shows a linear dependence on the applied electric field E, where d is the sample thickness, and t_{tr} is the transit time. The electron mobility μ is obtained from $v = \mu E$ [17]. The mobility of electrons at room temperature in CZT2 is about 337 ± 17 cm^2/Vs, which is much lower than that in CZT1 (848 ± 42 cm^2/Vs). It seems that lower electron mobility is corresponding to the higher density of donor and acceptor defects. In order to explain the effects of the total trap density on the carrier mobility, the scattering mechanisms were discussed, e.g., polar-optical phonon scattering, piezoelectric potential scattering, acoustic-mode (deformation potential) and scattering, ionized impurity scattering [8,18]. Neutral impurity scattering and structural defect (e.g., dislocations and stacking faults) scattering are also supposed to operate at low temperatures [19]. Theoretical estimation of the electron mobility in the high-purity material should consider the contributions from various scattering mechanisms.

Piezoelectric potential scattering occurs in crystals with zincblende structure [18]. The mobility of electrons due to the piezoelectric potential scattering, $\mu_{piezo} = 1.05 C_l \kappa_S^2 / e_{14}^2 (m*/m_0)^{3/2} T^{1/2}$, was estimated to be higher than 1.0×10^6 cm^2/Vs at room temperature [20], where C_l is the average longitudinal elastic coefficient, κ_S is the static dielectric constant, e_{14} is the piezoelectric coefficient, T is the absolute temperature, and $m* = 0.14 m_0$ is the effective mass of electrons, with m_0 being the electron's rest mass [21]. The mobility of electrons due to the acoustic phonon scattering, $\mu_{ac} = 3 \times 10^{-5} C_l / (m*/m_0)^{5/2} T^{3/2} E_{ac}^2$, was estimated to be about 2.1×10^4 cm^2/Vs in all the CZT crystals, where E_{ac} is the deformation potential. The effects of piezoelectric and deformation potential scattering on the room-temperature electron mobility were found to be negligible. The mobility of electrons due to the polar-optical phonon scattering is expressed as $\mu_{po} = (0.87/\alpha\hbar\omega_1)(m_0/m*)(\exp F - 1/F^{1/2}) \times G(F) e^{-\xi}$ [18]. The electron–phonon interaction can be handled in the weak-coupling approximation because the coupling constant α is 0.39 [8]. $F = \theta/T$, with θ being the Debye temperature. $\hbar\omega_1$ is the LO-phonon energy, and $G(F)e^{-\xi}$ is a function including screening effects. μ_{po} was estimated to be about 1183 cm^2/Vs in all the CZT crystals.

For ionized impurity scattering caused by ionized donor and acceptor defects, the Brooks–Herring (BH) formula based on the Born

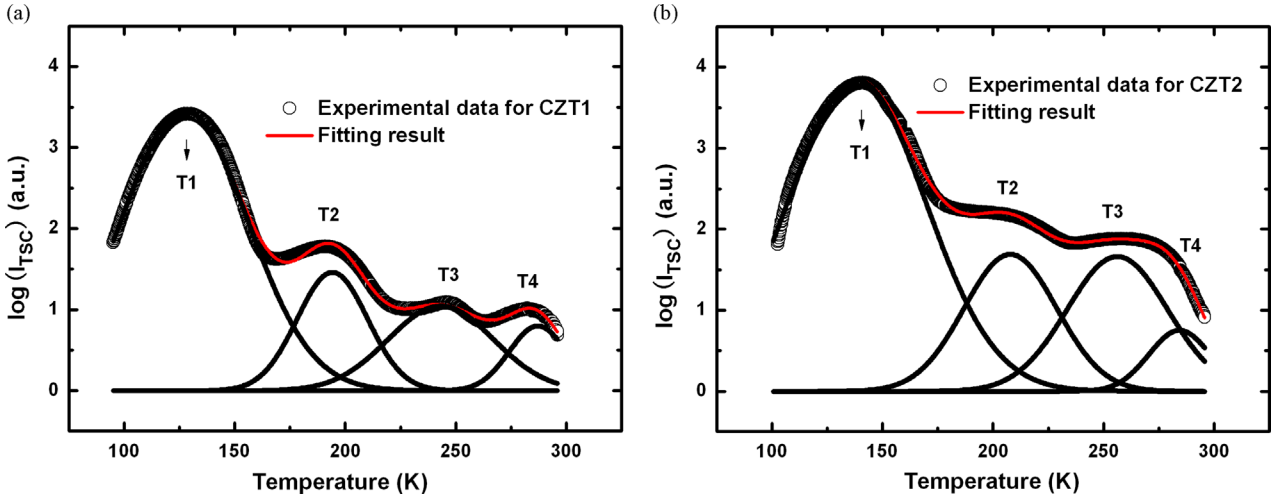

Fig. 1. The typical TSC spectra of CdZnTe single crystals (a) CZT1, (b) CZT2

Table 1
Trap densities (cm^{-3}) in CdZnTe single crystals.

	T1	T2	T3	T4
CZT1	$(1.21 \pm 0.06) \times 10^{16}$	$(6.25 \pm 0.31) \times 10^{15}$	$(1.46 \pm 0.07) \times 10^{15}$	$(4.56 \pm 0.23) \times 10^{13}$
CZT2	$(1.59 \pm 0.08) \times 10^{17}$	$(1.78 \pm 0.09) \times 10^{17}$	$(3.99 \pm 0.21) \times 10^{16}$	$(3.40 \pm 0.17) \times 10^{14}$

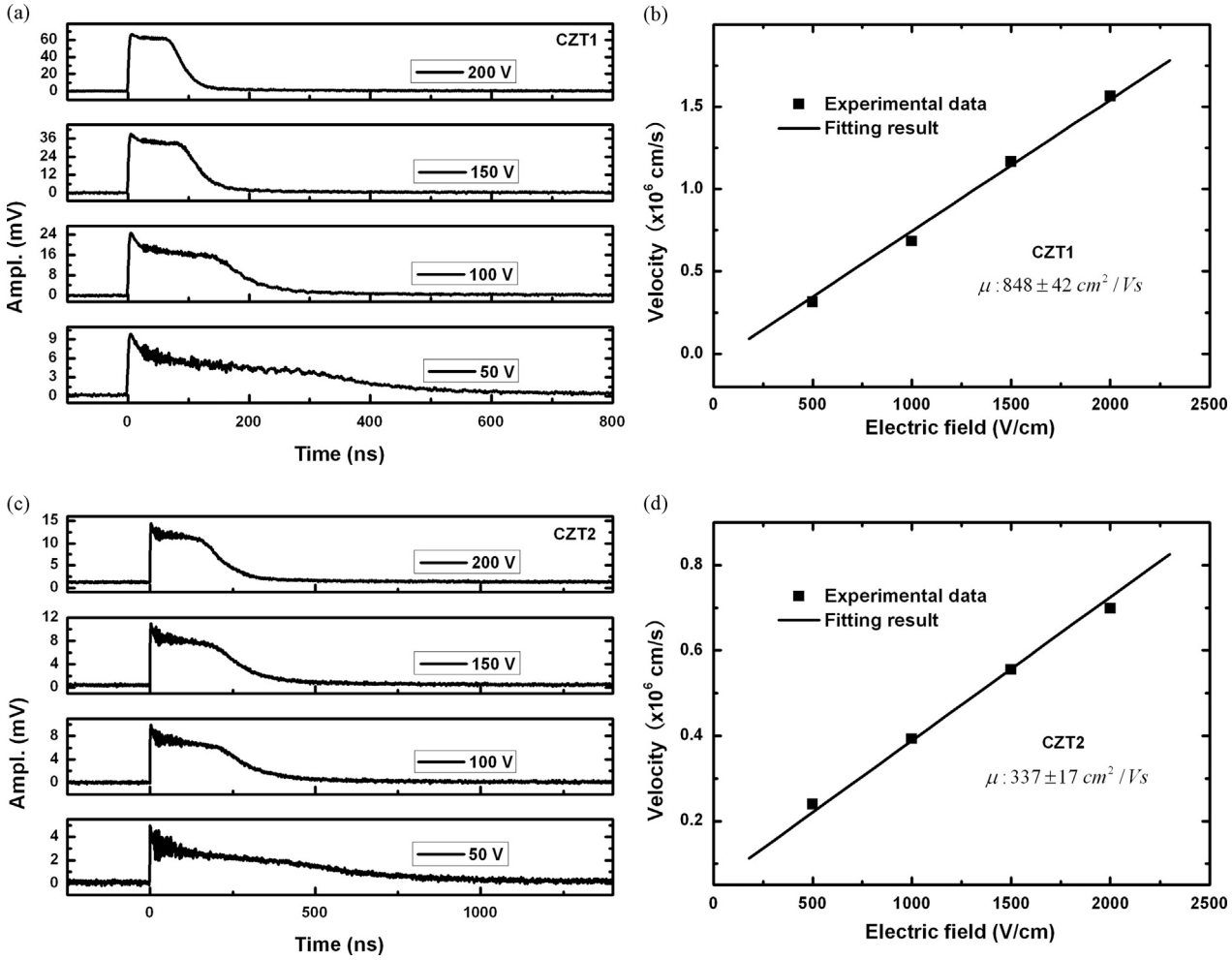

Fig. 2. TOF results, (a) and (c) are the typical transient current waveforms measured at different biases, (b) and (d) are the electric field strength dependence of the drift velocity of electrons

approximation was used [22]. The mobility of electrons due to the ionized impurity scattering is expressed as $\mu_{ii} = (64\varepsilon_s^2\pi^{1/2}(2k_BT)^{3/2})/(Z^2q^3N_I(m*)^{1/2}g(b))$, where ε_s is the dielectric permittivity, k_B is the Boltzmann's constant, and Z is the charge on the impurity defects in units of q, with q being the electron charge. $g(b) = \ln(1+b) - [b/(1+b)]$ is defined as the screening factor [23]. N_I is the total density of all the ionized impurity defects. It is assumed that all the impurity defects are fully ionized at room temperature. Thus, ionized impurity scattering mobility is inversely proportional to the total density of donor and acceptor defects $N_I = N_D^+ + N_A^- = N_D + N_A$, which could be determined from TSC results. For samples with the total trap density of about 2.0×10^{16} cm^{-3} (CZT1) and 3.8×10^{17} cm^{-3} (CZT2), μ_{ii} was estimated to be 9776 cm^2/Vs and 515 cm^2/Vs, respectively.

The total electron mobility μ is approximated by considering the contributions from various scattering mechanisms and is expressed as $(1/\mu) = (1/\mu_{piezo}) + (1/\mu_{ac}) + (1/\mu_{po}) + (1/\mu_{ii})$, according to Matthiesen's rule [18,24]. Fig. 3 shows the individual mobility due to each scattering mechanism and the total electron mobility as a function of the total density of donor and acceptor defects. For CZT1 and CZT2, μ was estimated to be 1004 cm^2/Vs and 352 cm^2/Vs, respectively. It is evident that theoretical estimations of electron mobility considering the contributions from a variety of scattering mechanisms are consistent with the experimental data in TOF results. There are two scattering mechanisms dominantly limiting the mobility of electrons in CdZnTe crystals at room temperature, i.e., polar-optical phonon scattering and ionized

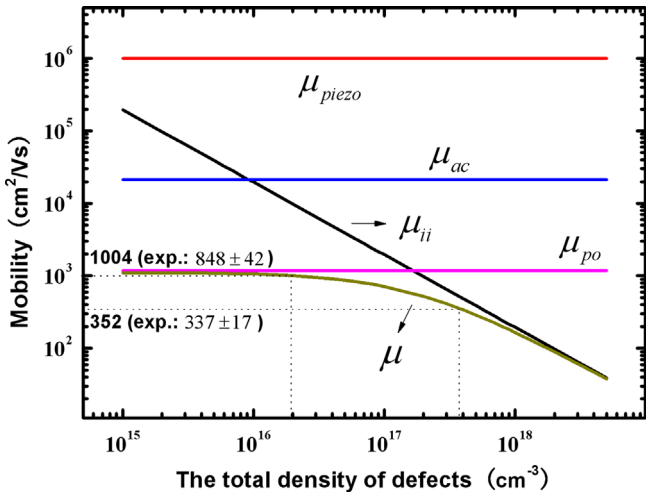

Fig. 3. The individual mobility due to each scattering mechanism and the total electron mobility at room temperature as a function of the total density of donor and acceptor defects

impurity scattering. With the total defect density lower than 1.0×10^{15} cm^{-3}, the electron mobility is determined by the polar-optical phonon scattering. As the density increases from 1.0×10^{15} cm^{-3} to 1.0×10^{17} cm^{-3}, the effects of the ionized impurity scattering on the mobility become more and more

dominating over polar-optical phonon scattering. With the total defect density higher than $1.0\times10^{17}\,cm^{-3}$, ionized impurity scattering will be the dominant scattering mechanism.

4. Conclusions

The effects of deep-level defects on the carrier mobility of $Cd_{0.9}Zn_{0.1}Te$:In single crystals were studied experimentally and theoretically. The total density of donor and acceptor defects in CZT1 is about $2.0\times10^{16}\,cm^{-3}$ and that in CZT2 is about $3.8\times10^{17}\,cm^{-3}$, as determined from TSC results. The mobility of electrons is about $848\pm42\,cm^2/Vs$ in CZT1 and $337\pm17\,cm^2/Vs$ in CZT2, as determined from TOF results. The individual mobility at room temperature due to piezoelectric potential, deformation potential and polar-optical phonon scattering was estimated to be 1.0×10^6, 2.1×10^4 and $1183\,cm^2/Vs$, respectively. The mobility due to ionized impurity scattering was estimated to be $9776\,cm^2/Vs$ in CZT1 and $515\,cm^2/Vs$ in CZT2. The total electron mobility, considering the contributions from a variety of scattering mechanisms, was estimated based on Matthiesen's rule to be $1004\,cm^2/Vs$ in CZT1 and $352\,cm^2/Vs$ in CZT2. Polar-optical phonon scattering was found to be the dominant scattering mechanism limiting the mobility at room temperature with the total defect density lower than $1.0\times10^{15}\,cm^{-3}$ in CZT crystals, and ionized impurity scattering will be the dominant with defect density higher than $1.0\times10^{17}\,cm^{-3}$.

Acknowledgments

This work was supported by the Special Fund of National Key Scientific Instruments and Equipments Development (2011YQ 040082), the National 973 Project of China (2011CB610400), the 111 Project of China (B08040), the National Natural Science Foundation of China (NNSFC-61274081, 51372205), the China Postdoctoral Science Foundation (2014M550509), the Doctorate Foundation of Northwestern Polytechnical University (CX201102), and Ministry of Education Fund for Doctoral Students Newcomer Awards of China. The authors would like to give special thanks to Dr. Nianxia Cao at Syracuse University for the great help during the paper writing.

References

[1] T. Schlesinger, J. Toney, H. Yoon, E. Lee, B. Brunett, L. Franks, R. James, Materials Science and Engineering: R: Reports 32 (2001) 103.
[2] R. James, B. Brunett, J. Heffelfinger, J. Van Scyoc, J. Lund, F. Doty, C. Lingren, R. Olsen, E. Cross, H. Hermon, Journal of Electronic Materials 27 (1998) 788.
[3] C. Szeles, Physica Status Solidi (B) 241 (2004) 783.
[4] K. Zanio, Cadmium Telluride, Semiconductors and Semimetals, vol. 13, Academic Press, New York, 1978.
[5] A. Castaldini, A. Cavallini, B. Fraboni, P. Fernandez, J. Piqueras, Journal of Applied Physics 83 (1998) 2121.
[6] M. Chu, S. Terterian, D. Ting, C. Wang, H. Gurgenian, S. Mesropian, Applied Physics Letters 79 (2001) 2728.
[7] V. Babentsov, J. Franc, R. James, Applied Physics Letters 94 (2009) 052102.
[8] K. Suzuki, S. Seto, T. Sawada, K. Imai, IEEE Transactions on Nuclear Science 49 (2002) 1287.
[9] M. Pavlović, U. Desnica, Journal of Applied Physics 84 (1998) 2018.
[10] G.A. Dussel, R.H. Bube, Physical Review 155 (1967) 764.
[11] Z.Q. Fang, D.C. Look, J. Zhao, Applied Physics Letters 61 (1992) 589.
[12] E. Lee, R. James, R. Olsen, H. Hermon, Journal of Electronic Materials 28 (1999) 766.
[13] L. Xu, W. Jie, G. Zha, Y. Xu, X. Zhao, T. Feng, L. Luo, W. Zhang, R. Nan, T. Wang, CrystEngComm 15 (2013) 10304.
[14] J. Francou, K. Saminadayar, J. Pautrat, Physical Review B 41 (1990) 12035.
[15] S.-H. Wei, S. Zhang, Physical Review B 66 (2002) 155211.
[16] A. Carvalho, A. Tagantsev, S. Öberg, P. Briddon, N. Setter, Physical Review B 81 (2010) 075215.
[17] C. Canali, M. Martini, G. Ottavian, K.R. Zanio, Physical Review B-Solid State 4 (1971) 422.
[18] W. Scott, Journal of Applied Physics 43 (1972) 1055.
[19] E.-K. Liu, B.-S. Zhu, J.-S. Luo, Semiconductor Physics, National Defense Industry Press, Beijing (1994) 369.
[20] B. Segall, R.E. Halsted, M.R. Lorenz, Physical Review 129 (1963) 2471.
[21] N. Krsmanovic, K. Lynn, M. Weber, R. Tjossem, T. Gessmann, C. Szeles, E. Eissler, J. Flint, H. Glass, Physical Review B 62 (2000) R16279.
[22] B.K. Ridley, Journal of Physics C-Solid State Physics 10 (1977) 1589.
[23] D. Chattopadhyay, H.J. Queisser, Reviews of Modern Physics 53 (1981) 745.
[24] M.B. Prince, Physical Review 92 (1953) 681.